THE UNIVERSITY *of* EDINBURGH

Edinburgh Research Explorer

Smooth and filamental structures in chaotically advected chemical fields

OPEN ACCESS

Smooth and filamental structures in chaotically advected chemical fields

Alexandra Tzella[*]

Laboratoire de Météorologie Dynamique, ENS, 24 rue Lhomond, F-75231 Paris, France

Peter H. Haynes

Department of Applied Mathematics and Theoretical Physics, University of Cambridge, CB3 0WA Cambridge, United Kingdom

This paper studies the spatial structure of decaying chemical fields generated by a chaotic-advection flow and maintained by a spatially smooth chemical source. Previous work showed that in a regime where diffusion can be neglected (large Péclet number), the structures are filamental or smooth depending on the relative strength of the chemical dynamics and the stirring induced by the flow. The scaling exponent, γ_q, of the qth-order structure function depends, at leading order, linearly on the ratio of the rate of decay of the chemical processes, α, and the average rate of divergence of neighboring fluid parcel trajectories (Lyapunov exponent), $\bar{h}$. Under a homogeneous stretching approximation, $\gamma_q/q = \max\{\alpha/\bar{h}, 1\}$ which implies that a well-defined *filamental-smooth transition* occurs at $\alpha = \bar{h}$. This approximation has been improved by using the distribution of finite-time Lyapunov exponents to characterize the inhomogeneous stretching of the flow. However, previous work focused more on the behavior of the exponents as q varies and less on the effects of α and hence the implications for the filamental-smooth transition. Here we set out the precise relation between the stretching rate statistics and the scaling exponents and emphasize that the latter are determined by the distribution of the finite-size (rather than finite-time) Lyapunov exponents. We clarify the relation between the two distributions. We show that the corrected exponents, $\tilde{\gamma}_q$, depend nonlinearly on α with $\tilde{\gamma}_q < \gamma_q$ for $\tilde{\gamma}_q < q$. The magnitude of the correction to the homogeneous stretching approximation, $\tilde{\gamma}_q - \gamma_q$, grows as α increases, reaching a maximum when the leading-order transition is reached ($\alpha = \bar{h}$). The implication of these results is that there is no well-defined bulk filamental-smooth transition. Instead it is the case that the chemical field is unambiguously smooth for $\alpha > h_{max}$, where h_{max} denotes the maximum finite-time Lyapunov exponent and unambiguously filamental for $\alpha < \bar{h}$, with an intermediate character for α between these two values. Theoretical predictions are confirmed by numerical results obtained for a linearly decaying chemistry coupled to a renewing type of flow together with careful calculations of the Crámer function.

PACS number(s): 47.52.+j, 47.70.Fw, 92.10.Lq, 47.51.+a

I. INTRODUCTION

It is now recognized that transport and stirring by chaotic advection in a smooth (differentiable) time-dependent incompressible flow is a problem that is relevant to a broad range of geophysical and engineering applications for which the flows are governed by their large-scale component [1]. In many of these applications, the advected concentration fields are not just passively advected but are chemically or biologically active. Important examples may be found in atmospheric chemistry (e.g., stratospheric ozone) and in marine ecosystems (e.g., interacting nutrient and plankton populations) where the biological population dynamics may be viewed as a kind of chemical reaction. More recent examples may be found in the areas of biofluidics and material processing (see, e.g., Ref. [2] and references therein).

Chaotic advection implies that nearby trajectories separate exponentially fast and conversely that fluid parcels originating in distant parts of the fluid are brought into close proximity, leading to rapid scalar mixing [3–5]. Through this processes of stirring, fluid elements are continually stretched, thinned, and folded, thereby converting scalar concentration fields to increasingly fine-scale filaments (or sheets). This

increasingly fine-scale structure will ultimately be dissipated by molecular diffusion, unless it is sustained by a source of large-scale scalar variability.

Filamental structures also underlie the spatial structures of concentration fields of chemically active scalars and are inherent to all the examples mentioned above. However the chemical dynamics can have an important influence on these structures. The simplest case for which this is true is the case of a linearly decaying chemical field, evolving in a closed domain, whose distribution is maintained at statistical equilibrium by a large-scale spatially smooth time-independent source. Of high relevance to a variety of physical problems, e.g., sea surface temperature [6], this problem has been examined for chaotic-advection flows with finite [7–12] and vanishing temporal correlation [13] and extended to include nonlinear chemical reactions of single and multiple chemical species described by ordinary [14,15] and delay differential equations [16–18]. In opposition to the effect of chaotic advection, the decaying chemical dynamics tend to relax the concentration fields toward the smooth spatial structure of the source. As the chemical reactions become stronger, a transition from a filamental to a smooth scaling behavior takes place [7].

A natural way to characterize the scaling behavior of the chemical fields is to consider statistical quantities such as structure functions, S_q, that describe the fluctuations of the

_____
[*]tzella@lmd.ens.fr

concentration fields. A theoretical prediction for the scaling exponents of S_q was deduced in Ref. [7] in which the main approximation made was the assumption that all infinitesimally small fluid elements stretch at the same rate, $\bar{h}$, whose value is given by the most positive Lyapunov exponent associated with the backward advection dynamics. This approximation, in this paper called the *homogeneous-stretching approximation*, led to the conclusion that, independent of the details of the flow motion, the scaling exponents should, at leading-order, depend linearly on both $\alpha/\bar{h}$ and the order of the structure function, q, where α denotes the rate of decay of the chemical processes. As a first approximation, the scaling exponents satisfy

$$\gamma_q = \max\{\alpha/\bar{h}, 1\}q, \qquad (1)$$

implying that a well-defined bulk *filamental-smooth transition* should occur when $\alpha = \bar{h}$.

A number of ensuing numerical studies performed for simple chaotic-advection flows and for chosen values of α suggested that as long as q is small, the theoretical prediction (1) should remain valid [9]. On the other hand, the higher-order structure functions were found to exhibit an anomalous behavior whereby their exponents were shown to depend nonlinearly on q [9–13]. This behavior was argued in Ref. [9] to be the direct consequence of the inhomogeneous stretching statistics of the flow. Employing a Cramér function to describe the distribution of finite-time stretching rates, Neufeld *et al.* [9] corrected the theoretical prediction (1). Nonetheless, Neufeld *et al.* [9] did not explore completely the effects of varying α on the behavior of the scaling exponents and therefore did not consider the full implications for the filamental-smooth transition.

Our main focus in this paper is to (i) understand how the scaling exponents vary as a function of the chemical decay rate and (ii) to re-examine the filamental-smooth transition. The expression for the scaling exponents of Ref. [9] is here rederived by refining the main assumptions from which they were derived. We note, following Ref. [10], that the distribution that governs the small-scale structure of the chemical fields is not the finite time but the *finite-size Lyapunov exponent distribution*. In Ref. [10] an *ad hoc* approximation was used to obtain the finite-size distribution in terms of the finite-time distribution. We examine this approximation carefully following the analogy of statistics of the first-passage times for random walks. The consequence of an inhomogeneous stretching distribution is that the homogeneous-stretching approximation is valid only for vanishingly small chemical decay ($\alpha \rightarrow 0$). We find that the corrected scaling exponents, $\tilde{\gamma}_q$, depend nonlinearly on α with $\tilde{\gamma}_q < \gamma_q$ for $\tilde{\gamma}_q < q$ with the corrections being most important when the homogeneous-stretching approximation [Eq. (1)] predicts a filamental-smooth transition ($\alpha = \bar{h}$). One implication is that there is no single well-defined bulk filamental-smooth transition.

The outline of the paper is as follows. Section II (complemented by Appendix, Secs. 1 and 2) consists of the theoretical part of the paper where following a careful examination of the finite-size exponent distribution, the expression for the scaling exponents is deduced and subsequently explored. To verify the theoretical predictions of Sec. II, we consider the example of a renewing type of flow, the widely employed (see, e.g., Ref. [19]) alternating sine flow. The comparison between theory and numerics is achieved by careful calculation of the Cramér function and thus also of the theoretical expression for the scaling exponents, in regions for which the stretching statistics are non-Gaussian. This method is described in Sec. III (complemented by Appendix, Sec. 3). The scaling exponents are subsequently calculated in the first part of Sec. IV. In the second part of Sec. IV, they are validated against the scaling exponents obtained from a set of numerical simulations performed for flows of various shear strength and a range of chemical decay rates, particularly those in the neighborhood of the transition predicted by the homogeneous stretching theory ($\alpha = \bar{h}$). The paper concludes with Sec. V.

II. THEORETICAL FORMULATION

A. Evolution equations and structure descriptions for chemical concentration fields

The spatial and temporal evolution of a passively advected chemically active concentration field, $c(\boldsymbol{x}, t)$, is described by the advection-diffusion-reaction (ADR) equations. Their general form is given by

$$\frac{\partial c(\boldsymbol{x}, t)}{\partial t} + \boldsymbol{v}(\boldsymbol{x}, t) \cdot \nabla c(\boldsymbol{x}, t) = \mathcal{F} + \kappa \nabla^2 c(\boldsymbol{x}, t), \qquad (2)$$

where κ is the molecular diffusion coefficient and $\boldsymbol{v}(\boldsymbol{x}, t)$ is assumed to be a large-scale velocity field that is incompressible and spatially smooth (i.e., $\nabla \cdot \boldsymbol{v} = 0$ and $|\nabla \boldsymbol{v}| < \infty$) varying on a scale, L_v, that we take as the unit length scale. We will consider flows that are random in time which have no transport barriers such that even if the velocity field is a smooth function of space, the Lagrangian trajectories are chaotic (see, e.g., Ref. [3]). To simplify the analysis, we will only consider two-dimensional flows. However, the theory is readily extendable to higher dimensions.

The forcing term $\mathcal{F}$ describes the chemical reactions as well as the effect of sources and sinks. We will here concentrate on a forcing term whose form is such that, in the absence of advection, Eq. (2) has a single stable fixed point (see Ref. [20] where a more complicated chemical behavior is explored). As it will be clear later, this stability is necessary for the chemical fields to reach a statistical equilibrium at sufficiently large t. Following previous investigations [7], we consider the simple example of a continually forced linearly decaying chemical field with

$$\mathcal{F} \equiv \alpha(\mathcal{F}_0(\boldsymbol{x}) - c), \qquad (3)$$

where $\mathcal{F}_0(\boldsymbol{x})$ is some spatially smooth source that introduces variability at some large scale, $L_{\mathcal{F}_0}$, that we again take as the unit length scale, i.e., the same length scale as that of the flow, and $\alpha > 0$ is the rate at which the chemical field relaxes toward this source. Note that the spatial dependence of the forcing term is crucial for the generation of a nontrivial spatial structure in the chemical field.

The main focus of this paper is to examine the scaling behavior of the chemical concentration field once this has reached a statistical equilibrium (the limit of $t \to \infty$). The local scaling behavior may be described in terms of the Hölder exponent, $\gamma(\boldsymbol{x})$, that characterizes the strength of the singularity of $c(\boldsymbol{x}, t)$ at a point $\boldsymbol{x}$. For an nondifferentiable (e.g., filamental) field $\gamma(\boldsymbol{x})$ satisfies

$$|c(\boldsymbol{x} + \delta\boldsymbol{x}, t) - c(\boldsymbol{x}, t)| \sim \delta x^{\gamma(\boldsymbol{x})}, \quad \delta x \ll 1, \quad (4)$$

with $0 < \gamma < 1$ while for a smooth (i.e., differentiable) field $\gamma = 1$. Note that $\delta x \equiv |\delta\boldsymbol{x}|$. The average scaling behavior of $c(\boldsymbol{x}, t)$ may be described in terms of the structure functions defined for $q > 0$ as

$$S_q(\delta\boldsymbol{x}) \equiv \lim_{t \to \infty} \langle |c(\boldsymbol{x} + \delta\boldsymbol{x}, t) - c(\boldsymbol{x}, t)|^q \rangle, \quad (5)$$

where $\langle \ldots \rangle$ denotes a spatial average over the local scaling behavior of the field. For small length scales, $S_q(\delta\boldsymbol{x})$ typically exhibits a power-law behavior such that

$$S_q(\delta\boldsymbol{x}) \sim \delta x^{\gamma_q}, \quad \delta x \ll 1, \quad (6)$$

where γ_q is the qth order scaling exponent, satisfying $0 \leq \gamma_q \leq q$.

B. Scaling behavior: From local to global

For cases for which advective transport dominates diffusion, i.e., large Péclet number, a natural approach is to set $\kappa = 0$. In this case, the chemical evolution of any fluid parcel is independent of the rest of the parcels that constitute the fluid (see, e.g., Ref. [7]). Equation (2) is thus reduced into a low-dimensional dynamical system, given by

$$\frac{dC_{X(t)}(t)}{dt} = \mathcal{F}(C_{\mathbf{X}(t)}(t), X(t)), \quad (7a)$$

$$\frac{dX(t)}{dt} = \boldsymbol{v}(X(t), t), \quad (7b)$$

where $X(t)$ denotes the fluid parcel's trajectory and $C_{X(t)}(t)$ is its chemical concentration, satisfying $C_{X(t)}(t) = c(\boldsymbol{x} = X(t), t)$. Note that the neglect of diffusion means that any predictions concerning the spatial structure of the chemical field apply only above a certain spatial cut-off scale whose value approaches zero for smaller and smaller diffusivities (see Ref. [21] where this argument is developed for a linearly decaying chemical field).

The concentration difference between two points can therefore be estimated by considering the concentration difference between two neighboring fluid parcels with

$$c(\boldsymbol{x} + \delta\boldsymbol{x}, t) - c(\boldsymbol{x}, t) = C_{X(t)+\delta X(t)}(t) - C_{X(t)}(t) \equiv \delta C_{\delta X(t); X(t)}(t). \quad (8)$$

The asymptotic behavior of $\delta C_{\delta X(t); X(t)}(t)$, denoted by δC_∞, can be obtained by using the variation of constants formula (see, e.g., Ref. [22]), taking into account the source term (3),

$$\delta C_\infty = \int_0^\infty e^{-\alpha t} \delta_X \mathcal{F}_0(-t) dt, \quad (9)$$

where $\delta_X \mathcal{F}_0(t) \equiv \mathcal{F}_0(X(t) + \delta X(t)) - \mathcal{F}_0(X(t))$. Note that for ease of notation we have suppressed $\{\delta x = \delta X(0); \ \boldsymbol{x} = X(0)\}$, the label for the concentration difference at the final time that for convenience of notation we have taken to be $t = 0$.

An approximate expression for $\delta_X \mathcal{F}_0(t)$ can be obtained by first noting that because the source depends smoothly on space, $\delta_X \mathcal{F}_0(-t) \sim \delta X(-t) \equiv |\delta X(-t)|$ for $\delta X(-t) \ll L_{\mathcal{F}_0} = 1$. An expression for $\delta X(-t)$ in terms of δx can be obtained by linearizing Eq. (7b) from where it is found that the evolution of $\delta X(-t)$ is dictated by a set of (two in the case of a two-dimensional flow) exponentials whose exponents determine the rate of growth of $\delta X(-t)$ (or rate of decrease if δx is oriented along the contracting direction). The value of these exponents are closely related to the (infinite-time) Lyapunov exponents, the largest of which is defined by

$$\bar{h} = \lim_{t \to \infty} h_t(\boldsymbol{x}) = \lim_{t \to \infty} \lim_{\delta x \to 0} \frac{1}{t} \ln \frac{\delta X(-t)}{\delta x}, \quad (10)$$

where $h_t(\boldsymbol{x})$ is the finite-time Lyapunov exponent (FTLE) (see, e.g., Ref. [23]). The value of $h_t(\boldsymbol{x})$ depends on the initial condition, in this case the final ($t = 0$) fluid parcel position $\boldsymbol{x}$. The Oseledec multiplicative ergodic theorem [24] states that, as long as the flow is ergodic, the value of $\bar{h}$ is independent of $\boldsymbol{x}$, thus allowing the system to be globally characterized.

The exponential increase of $\delta X(-t)$ can be valid only for the time period for which $|\delta X(-t) \ll L_v = 1$. For larger length scales, linearizing Eq. (7b) is no longer valid and finite-size effects become important. At the same time, at these length scales, $\delta X(-t) \sim L_{\mathcal{F}_0}$ and thus the value of $\delta_X \mathcal{F}_0(-t)$ saturates. It follows that qualitatively,

$$\delta_X \mathcal{F}_0(-t) \sim \min\{\delta X(-t), 1\}. \quad (11)$$

The time it takes for $\delta_X \mathcal{F}_0(-t)$ to saturate is equal to the time it takes for $\delta X(-t)$ to exit the exponential regime and varies with the pair's final position and orientation. To calculate this time, it is useful to define the *stir-down time*, $T_{\delta x}(\boldsymbol{x})$, as the time it takes for $\delta X(-t)$, initially with value δx, to *first* reach $L_v = 1$. We may thus express the rate of growth of $X(-t)$ from δx to 1 in terms of $T_{\delta x}(\boldsymbol{x})$ as

$$h_{\delta x}(\boldsymbol{x}) = \frac{1}{T_{\delta x}(\boldsymbol{x})} \ln \frac{1}{\delta x}, \quad \delta x \ll 1, \quad (12)$$

which we define as the finite-size Lyapunov exponent (FSLE). We use this term following Refs. [25,26] though they focused on its ensemble average [42].

Once we have substituted expression (11) into (9), we can deduce that for $\delta x \ll 1$, the integral of Eq. (9) is dominated by the maximum value of its integrand whose value and location depend on whether α is larger or less than $h_{\delta x}$. If $\alpha > h_{\delta x}$, the maximum occurs at $t = 0$ while if $\alpha < h_{\delta x}$, the maximum occurs at $t = T_{\delta x}$. Thus,

$$\delta C_\infty(\delta x) \sim \delta x^{\min\{\alpha/h_{\delta x}, 1\}}, \quad \delta x \ll 1, \tag{13}$$

in all but the direction the filaments grow, in which case, $h_{\delta x} < 0$ and $\delta C_\infty \sim \delta x$ for all α. We may therefore conclude that the nature of the local scaling behavior of the field, smooth or filamental, where a filamental field is defined [7] to be nondifferentiable in all but one directions, depends on the ratio of α to $h_{\delta x}$.

The qth-order stationary-state structure function, S_q, may now be obtained by averaging the local scaling behavior [Eq. (13)] over the ensemble of fluid parcel pairs that constitute the flow. Since the pairs' final positions and orientations are arbitrarily chosen, a probability density function (*pdf*) for the finite-size Lyapunov exponent, $Q(h, \delta x)$, can be defined such that $Q(h, \delta x)dh$ is the probability that $h_{\delta x}$ lies between h and $h + dh$. Thus,

$$S_q(\delta x) \sim \int_0^{h_{\max}} \delta x^{\min\{q\alpha/h, q\}} Q(h, \delta x) dh, \quad \delta x \ll 1, \tag{14}$$

where, because $|\nabla \boldsymbol{v}| < \infty$, the value of $h_{\max}$ is finite. Note that within the homogeneous-stretching approximation, $Q(h, \delta x) = \delta(h - \bar{h})$ from where expression (1) for γ_q is obtained.

C. Finite-size versus finite-time statistics

The *pdf* for the FTLEs [see Eq. (10)], denoted by $P(h, t)$, can be approximated using *large-deviation theory* [27] and is given by

$$P(h, t) \propto e^{-G(h)t}, \quad \text{as } t \to \infty, \tag{15a}$$

where $G(h)$ is the Crámer function [28] (also called the entropy function—see Ref. [29] for a detailed presentation). Fully encapsulating the stretching statistics of the flow, $G(h)$ is a time-independent positive convex function with a quadratic minimum at $\bar{h}$, i.e.,

$$G(\bar{h}) = G'(\bar{h}) = 0 \text{ and } G(h) \geq 0, \ G''(h) > 0, \tag{15b}$$

where $\bar{h}$ is both the mean of the distribution as well as the (infinite-time) Lyapunov exponent of the flow. The quadratic minimum corresponds to a Gaussian behavior for $P(h, t)$, a consequence of the central limit theorem. Far from this minimum, the form of $G(h)$ depends on the details of the stretching statistics of the flow. With the exception of a small number of special cases there exists no analytical expression for $G(h)$. In general $G(h)$ has to be estimated numerically (see Sec. III for more details).

No corresponding expression for $Q(h, \delta x)$, the *pdf* for the

FSLEs, has been obtained. An *ad hoc* approximation for $Q(h, \delta x)$ was given by Boffetta *et al.* [10]. This approximation, which we denote by $Q_0(h, \delta x)$, is based on (i) approximating the stir-down time by $T_{\delta x} \sim \frac{1}{h}\ln(1/\delta x)$ and (ii) using $T_{\delta x}$ for t in Eq. (15). This results in

$$Q_0(h, \delta x) = P\left(h, \frac{1}{h}\ln(1/\delta x)\right), \tag{16a}$$

from where it may be deduced that

$$Q_0(h, \delta x) \propto \delta x^{G(h)/h} h^{-1/2}. \tag{16b}$$

However it is difficult to justify this approximation in any formal way. For example, $P(h, t)$ is a *pdf* at a fixed t while $Q(h, \delta x)$ is a *pdf* at a fixed δx.

To examine more carefully the *ad hoc* approximation (16), it is useful to consider the analogous problem of a particle undergoing a general random walk. Let $p(z, t)$ denote a *pdf* such that $p(z, t)dz$ is the probability that the particle is within the interval $[z, z + dz]$ at time t, given that it was at $-z_0 < 0$ at time $t = 0$. Let $q_0(t)$ denote the *pdf* associated with the first-passage-time probability, i.e., $q_0(t)\delta t$ is the probability that the particle attains the origin for the first time during the interval $[t, t + dt]$.

An exact relation exists between $p(0, t)$ and $q_0(t)$, given by

$$p(0, t) = \int_0^t q_0(t') p_0(t - t') dt', \tag{17}$$

where $p_0(t)$ denotes the *pdf* of the particle position at time t, released at $z = 0$ and evaluated at $z = 0$ (see, e.g., Ref. [30]). Using this relation, we can deduce (see Appendix, Sec. 1 a) that the large-t behavior of $q_0(t)$ satisfies at leading order,

$$q_0(t) \propto \exp[- tG(z_0/t)], \quad \text{for } z_0 \text{ large} \tag{18a}$$

$$\sim p(0, t), \tag{18b}$$

where the large deviation form for $p(0, t)$ was used [see Eq. (15) but now applied to the random walk].

Determining $Q(h, \delta x)$ is analogous to determining the distribution of the particle's average velocity over the period until it first visits $z = 0$. Let this velocity be denoted by $V(t)$. Its distribution, $Q(v, z_0)$, can be obtained from $q_0(t)$ by a change of variables, $V(t) = z_0/T$, where T denotes the first-passage time. Determining $P(h, t)$ is analogous to determining the distribution of the average particle velocity (averaged over all times prior to t). Let this velocity be denoted by $U(t)$. Its distribution, denoted by $P(u, t)$, can be obtained from $p(z, t)$ by a change of variables $U(t) = (Z(t) + z_0)/t$. It follows that

$$
\begin{aligned}
Q(v, z_0) &= z_0/v^2 q_0(t = z_0/v) \\
&\sim z_0/u^2 p(0, z_0/u), \quad \text{where from Eq. (18), } t = z_0/u \text{ and } u = v \text{ with } z_0 \gg 0 \\
&= 1/u P(u, z_0/u), \quad \text{and from Eq. (16a),} \\
&\propto Q_0(v, z_0).
\end{aligned} \tag{19}
$$

In other words, for $z_0 \gg 0$, i.e., $\delta x \ll 1$, the *ad hoc* approximation (16) for the finite-size distribution is up to a factor correct. For a particle undergoing a simple random walk with a constant drift and diffusion (an example that is relevant for the isotropic Kraichnan flow), $Q \equiv Q_0$ and thus in this case, the *ad hoc* approximation (16) is exact (see Appendix, Sec. 1 b).

D. Scaling exponents and filamental-smooth transition

Substituting the approximate expression (16) for $Q(h, \delta x)$ into Eq. (14), the qth-order structure function may now be expressed as a sum of two integrals:

$$S_q(\delta x) \propto \left[\int_0^\alpha \delta x^{f(h)} h^{-1/2} dh + \int_\alpha^{h_{max}} \delta x^{g(h)} h^{-1/2} dh \right], \tag{20}$$

where the first and second integrals denote, respectively, the parts of the distribution that contribute to a smooth and a filamental behavior for $c(\mathbf{x}, t)$. The functions f and g are equal to

$$f(h) = G(h)/h + q, \tag{21a}$$

$$g(h) = (G(h) + q\alpha)/h \tag{21b}$$

and have the following stationary points

$$f'(\bar{h}) = 0 \Rightarrow G'(\bar{h})\bar{h} = G(\bar{h}), \tag{22a}$$

$$g'(h_{q\alpha}) = 0 \Rightarrow G'(h_{q\alpha})h_{q\alpha} = G(h_{q\alpha}) + q\alpha, \tag{22b}$$

where to deduce Eq. (22a), we invoke the properties of $G(h)$ [see Eq. (15b)]. A small amount of simple algebra is needed to show that $\bar{h}$ and $h_{q\alpha}$ are both unique stationary points at which the global maximum of $-f(h)$ and $-g(h)$ is, respectively, attained. It is useful to understand where the value of $h_{q\alpha}$ lies relative to $\bar{h}$. Differentiating Eq. (22b) with respect to $q\alpha$,

$$dh_{q\alpha}/d(q\alpha) = (G''(h_{q\alpha})h_{q\alpha})^{-1} > 0 \tag{23}$$

the inequality a result of $G'' > 0$. Thus, for all $\alpha q > 0$, $h_{q\alpha}$ satisfies $h_{q\alpha} > \bar{h}$ with

$$\lim_{q\alpha \to 0} h_{q\alpha} = \bar{h}. \tag{24}$$

Note that since h_{max} is the supremum of h_{qa},

$$\lim_{q\alpha \to \infty} h_{q\alpha} = h_{max}. \tag{25}$$

An expression for $\tilde{\gamma}_q$, the scaling exponents of $S_q(\delta x)$, can be obtained using Laplace's method on Eq. (20), valid for $\delta x \ll 1$, from where we deduce that (see also Ref. [9])

$$\tilde{\gamma}_q = \min\{q, G'(h_{q\alpha})\}, \text{ with } G'(h_{q\alpha}) = (G(h_{q\alpha}) + q\alpha)/h_{q\alpha}. \tag{26}$$

Note that for $\alpha > h_{max}$, $\tilde{\gamma}_q = q$ for all q. Note also that $\tilde{\gamma}_q > q\alpha/h_{max}$. Expression (26) is identical to the expression

obtained in Ref. [9]. However the approach is different: While Neufeld *et al.* [9] focus on the inhomogeneities of $P(h, t)$ as $t \to \infty$, in particular taking into account the fractal dimension of those sets of $h_t(\mathbf{x})$ that take different values from $\bar{h}$ as $t \to \infty$, our focus, as well as that of Boffetta *et al.* [10], is on the distribution of the recent stretching history, as given by $Q(h, \delta x)$.

Based on the properties of $G(h)$, we now examine the general behavior of $\tilde{\gamma}_q$ as a function of α and q and compare it to the behavior of γ_q, where γ_q is given by Eq. (1). The homogeneous-stretching approximation is only valid in the limit of $q\alpha \to 0$ in which $h_{q\alpha} = \bar{h}$ and

$$\lim_{q\alpha \to 0} \tilde{\gamma}_q = \gamma_q. \tag{27}$$

However, as the values of either α or q increase, the correction to the homogeneous-stretching approximation, defined by $\varepsilon(q, \alpha) \equiv \gamma_q - \tilde{\gamma}_q$, becomes important.

1. Varying α

To understand how $\varepsilon(q, \alpha)$ varies with α, consider the case of $\alpha < \alpha_q^*$, where α_q^* is defined as the smallest value of α for which $\tilde{\gamma}_q = q$, i.e., the value of α for which $G'(h_{q\alpha}) = q$. Using Eq. (23), the behavior of $\partial \varepsilon / \partial \alpha$ as α varies ($q > 0$) is given by

$$\frac{\partial \varepsilon(q, \alpha)}{\partial \alpha} = \begin{cases} q(1/\bar{h} - 1/h_{q\alpha}) > 0, & \text{for } 0 < \alpha < \bar{h} \\ -q/h_{q\alpha} < 0, & \text{for } \bar{h} \le \alpha < \alpha_q^*. \end{cases} \tag{28}$$

A key point necessary to deduce Eq. (28) is that $\varepsilon(q, 0) = 0$ and thus for all $\alpha < \bar{h}$, $\varepsilon > 0$, and $\tilde{\gamma}_q < \gamma_q$. Therefore, the smallest value of $\alpha > 0$ that satisfies $\tilde{\gamma}_q = 0$ must be larger than $\bar{h}$, i.e.,

$$\alpha_q^* > \bar{h}, \text{ for all } q > 0, \tag{29}$$

with $\alpha_0^* = \bar{h}$. Consequently, $\varepsilon(q, \alpha)$ increases as α increases, reaching a global maximum when $\alpha = \bar{h}$; the value for which the homogeneous-stretching approximation predicts a bulk filamental-smooth transition to take place. Thereafter, its value decreases until $\alpha = \alpha_q^*$ when it becomes equal to 0. It thus follows that for $0 < \alpha < \alpha_q^*$, $\tilde{\gamma}_q$ is a nonlinear monotonically increasing concave function of α that satisfies $\tilde{\gamma}_q < q$.

We may thus conclude that the transition from a filamental to a smooth field behavior is smooth, not sharp as predicted by the homogeneous-stretching approximation [see Eq. (1)]. Moreover, the value of α_q^* varies with q. In particular, from Eq. (22b), it can be deduced that for all $q > q'$,

$$\alpha_q^* > \alpha_{q'}^*, \tag{30}$$

with $\lim_{q \to \infty} \alpha_q^* = h_{max}$. It follows that while we can say that for $\alpha \le \bar{h}$, all $S_q(\delta x) \sim \delta x^{\tilde{\gamma}_q}$ are nondifferentiable (i.e., $\tilde{\gamma}_q < q$) and for $\alpha > h_{max}$, all $S_q(\delta x)$ are smooth (i.e., $\tilde{\gamma}_q = q$), the nature of $S_q(\delta x)$ depends on the value of q for α in between $\bar{h}$ and h_{max}. The latter is a direct consequence of the dependence of α_q^* on q.

Neufeld *et al.* [9] on the other hand argued that a bulk filamental-smooth transition should take place at $\alpha = \bar{h}$. To deduce this, Neufeld *et al.* [9] used as diagnostic the maximum of the fractal dimensions, $D_{\max}$, of the singular sets of FTLEs that in the limit of $t \to \infty$ are larger than α. They showed that while for $\alpha \geq \bar{h}$, $D_{\max} < 2$, for $\alpha < \bar{h}$, $D_{\max} = 2$, i.e., the singular structures become space-filling. This change in behavior is reflected in the behavior of $\widetilde{\gamma}_q$ which for $\alpha < \bar{h}$ satisfies $\widetilde{\gamma}_q < q$ for all $q > 0$. However, such a change would be very difficult to observe from the chemical fields: even if they are not space-filling, the singular sets in the chemical field exist for $\alpha > \bar{h}$ and contribute to the value of $\widetilde{\gamma}_q$. The result is that the transition from smooth to filamental essentially takes place over some finite range of α. Results presented in Sec. IV B demonstrate this point.

2. Varying q

Now consider how $\varepsilon(q, \alpha)$ varies with q. Two cases are distinguished: (i) $\alpha \leq \bar{h}$ and (ii) $\bar{h} < \alpha < h_{\max}$. For case (i), $\widetilde{\gamma}_q < q$ and since $\partial \varepsilon / \partial q > 0$, the difference between γ_q and $\widetilde{\gamma}_q$ increases as q increases. $\widetilde{\gamma}_q$ is a nonlinear monotonically increasing function of q. For case (ii), there exists a q_0 such that $\alpha = \alpha_{q_0}^*$. From Eq. (30) we can deduce that for $q > q_0$, $\alpha_q^* > \alpha_{q_0}^* = \alpha$. Conversely, for $q \leq q_0$, $\alpha = \alpha_{q_0}^* \geq \alpha_q^*$. Therefore,

$$\widetilde{\gamma}_q = q, \quad \text{for } q \leq q_0, \tag{31a}$$

$$\widetilde{\gamma}_q < q, \quad \text{for } q > q_0, \tag{31b}$$

and thus as q increases the structure functions are initially smooth up until q_0 after which they become nondifferentiable, implying a filamental behavior for $c(\mathbf{x}, t)$. Since $\alpha_0^* = \bar{h}$ and $\lim_{q \to \infty} \alpha_q^* = h_{\max}$, it is easy to deduce that when $\alpha = \bar{h}$, $q_0 = 0$ (i.e., $\widetilde{\gamma}_q \leq q$ for all q) while as $\alpha \to h_{\max}^-$, $q_0 \to \infty$ (i.e., $\widetilde{\gamma}_q = q$ for all q). It is possible to obtain an expression for the large-q behavior of $\widetilde{\gamma}_q$. For $\alpha < h_{\max}$, this is given by (see Appendix, Sec. 2)

$$\widetilde{\gamma}_q \sim \frac{\alpha q}{h_{\max}}, \quad \text{as } q \to \infty. \tag{32}$$

Note that this expression corrects expression (4.15) in Neufeld *et al.* [9].

III. EVALUATING THE SCALING EXPONENTS

In order to verify the theoretical predictions of Sec. II an accurate evaluation of $G(h)$ is necessary. Since $h_{q\alpha}$ satisfies $h_{q\alpha} \geq \bar{h}$, this evaluation is particularly important for $h \geq \bar{h}$.

Care is needed in finding an accurate estimate of $G(h)$ outside the neighborhood of $\bar{h}$. The traditional method employed [31,32] depends on determining the distribution of h at a given time t through sampling of a large number of stretching realizations. Thereafter, using expression (15), $G(h)$ is estimated. Such a method allows only a part of the function to be calculated with confidence. This part is associated with the values of h that are frequently realized, i.e.,

those values that lie in the neighborhood of $\bar{h}$ where $G(h)$ is well approximated by a parabola, and $P(h, t)$, the finite-time Lyapunov exponent distribution, is Gaussian. Away from this neighborhood, the values of h occur scarcely, rendering an accurate estimate of $G(h)$ difficult to secure. Nevertheless, as either α or q increase, it is these infrequently realized values of h that dominate the scaling behavior of the field. The larger the value of α or q is, the larger and thus the more infrequent the dominant $h_{q\alpha}$ is, leading to an increasingly unreliable estimate for $G(h_{q\alpha})$.

In order to correctly calculate $\widetilde{\gamma}_q$ for any value of α or q, a more reliable method for calculating $G(h)$ is necessary. Recently, Haynes and Vanneste [33] developed such a method which has recently been refined in Vanneste [34] and successfully tested it for two-dimensional spatially homogeneous random-in-time chaotic-advection flows; both for Kraichnan [35] (vanishing temporal correlation with infinite $\nabla \mathbf{v}$) and for renewing (finite temporal correlation with $\nabla \mathbf{v} < \infty$). The basis of this method relies on determining $\Lambda(\sigma)$, a function closely related to the Legendre transform of $G(h)$, via an eigenvalue problem. Unlike previous methods, this one is not so strongly dependent on the numerical realization of infrequent random events and thus should enable a more accurate determination of $G(h)$ for a larger range of values of h.

The function $\Lambda(\sigma)$ is defined as

$$\Lambda(\sigma) \equiv \inf_{\widetilde{h}} \{(\sigma + 1)\widetilde{h} + G(\widetilde{h})\} = -hG'(h) + G(h),$$

$$\text{with } \sigma = -[1 + G'(h)], \tag{33}$$

where up to a shift and a change of sign it is the Legendre transform of $G(h)$, also known [36] as the free energy. $\Lambda(\sigma)$ satisfies $\Lambda'(\sigma) = h$ with $\Lambda''(\sigma) = -1/G''(h) < 0$. For incompressible two-dimensional flows, $\Lambda(\sigma) = \Lambda(-\sigma)$ and therefore $\Lambda(\sigma)$ has its maximum point at $\sigma = 0$. Using Eq. (33), it can also be deduced that $\Lambda(-1) = 0$ with $\Lambda'(-1) = \bar{h}$ (see Ref. [33]). The method for calculating Λ is given in Appendix, Sec. 3.

$\widetilde{\gamma}_q$ may be directly expressed in terms of Λ. Eq. (26) for the scaling exponents becomes

$$\widetilde{\gamma}_q = \min\{q, -1 - \sigma_q\} \quad \text{with } \Lambda(\sigma_q) = -\alpha q. \tag{34}$$

Two values of interest are here presented in order to introduce the notation:

$$\widetilde{\gamma}_1 = 0 \Rightarrow \sigma_1 = -1 \Leftrightarrow \alpha = 0,$$

$$\widetilde{\gamma}_1 = 1 \Rightarrow \sigma_1 = -2 \Leftrightarrow \alpha = \alpha_1^*.$$

IV. NUMERICAL RESULTS FOR AN EXAMPLE FLOW

A. Scaling exponents

$\Lambda(\sigma)$ is here determined for a particular type of renewing flow, the alternating sine flow, first introduced by Pierrehumbert [19] and widely employed by, among others, Neufeld *et al.* [7] and Birch *et al.* [15]. The calculation of $G(h)$ follows. The scaling exponents, $\widetilde{\gamma}_q$, are then evaluated as a
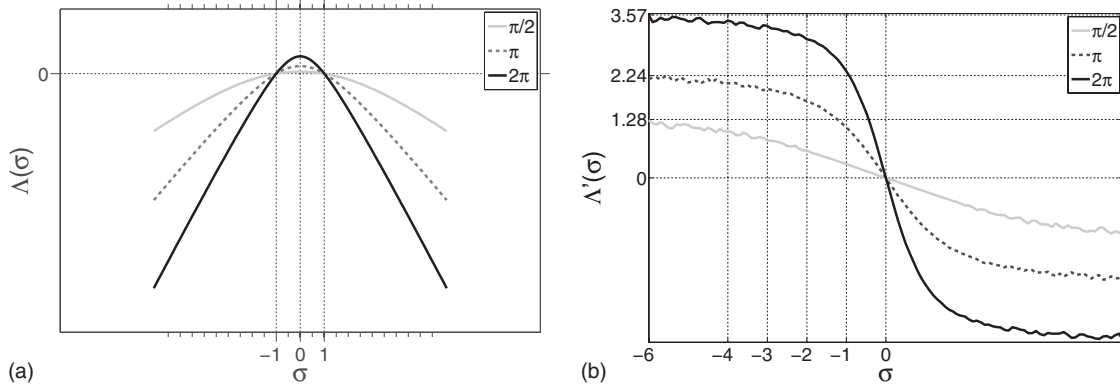
FIG. 1. (a) The function $\Lambda(\sigma)$ corresponding to the alternating sine flow [Eq. (36)] for $A = \pi/2$, π, and 2π (where $A = \pi U \tau$, $\tau = 1$ and U varies). (b) The corresponding derivative of $\Lambda(\sigma)$.

function of α and q. Their values are compared to γ_q, the homogeneous-stretching approximation for the scaling exponents [see Eq. (1)] as well as $\tilde{\gamma}'_q$, the exponents calculated from Eq. (26) using a quadratic approximation for $G(h)$, given by

$$G(h) = \frac{(h - \bar{h})^2}{4D}, \tag{35a}$$

leading to

$$\tilde{\gamma}'_q = \frac{\bar{h}}{2D}\left(\left[1 + \frac{4Dq\alpha}{\bar{h}^2}\right]^{1/2} - 1\right), \tag{35b}$$

where D is a constant. Note that for an isotropic Kraichnan flow, for which ∇v is infinite, expression (35a) is exact once $D = \bar{h}/d$, d being the dimension of the flow [35]. These com-

parisons are necessary to see the limitations of previous calculations, thus providing a link with the past literature [9–12].

The alternating sine flow is a purely strain flow with velocity field given by

$$v(x,t) = \begin{bmatrix} \Theta(\tau/2 - t \bmod \tau)U\sin(2\pi y + \phi_1) \\ \Theta(t \bmod \tau - \tau/2)U\sin(2\pi x + \phi_2) \end{bmatrix}, \tag{36}$$

where U controls the strength of the shear and $\Theta(t)$ is the Heaviside step function defined to be unity for $t \geq 0$ and zero otherwise. ϕ_1 and ϕ_2 are independent random angles uniformly distributed in $[0, 2\pi]$ whose value changes at each period τ in order to eliminate the presence of transport barriers in the flow.

Let $\psi_{-\tau}$ be the time-τ map of the flow such that $X(t-\tau) = \psi_{-\tau}X(t)$. Then, $\delta X(t-\tau) = S_{-\tau}\delta X(t)$ where

$$S_{-\tau} = \nabla\psi_{-\tau}|_{X=0} = \begin{pmatrix} 1 & -A\cos\phi_1 \\ -A\cos(A\sin\phi_1 + \phi_2) & 1 + A^2\cos(A\sin\phi_1 + \phi_2)\cos\phi_1 \end{pmatrix}, \tag{37}$$

with $A = \pi U \tau$.

A useful estimate was deduced for the (infinite-time) Lyapunov exponent, $\bar{h}$ by [15]. This is given by

$$\bar{h} \approx \frac{1}{\tau}\ln(1 + A^2/5 + 4A^4/67). \tag{38}$$

A theoretical upper bound for the value of h_{max} can be derived by determining the largest eigenvalue of $S_{-\tau}$. It follows that

$$h_{max} < \frac{1}{2\tau}\ln(1 + 3A^2 + A^4). \tag{39}$$

In practice, the upper bound of h_{max} is a good estimate for h_{max}. It turns out that this is because the value of A is the

same in the x and y directions. If the value of A is different, the upper bound of h_{max} is no longer a good estimate for h_{max} (for a detailed discussion see Ref. [34]).

To determine Λ, an ensemble of matrices $S_{-\tau}$ of size 10^5 (obtained by varying ϕ_1 and ϕ_2) and a set of 1000 line elements with orientation θ uniformly distributed in $[0, 2\pi]$ is considered. The resulting curve for $\Lambda(\sigma)$ obtained for σ varying in step-size 0.1, is displayed for three values of A in Fig. 1(a). This result was found to be robust for the range of values of σ shown, once compared to individual values of $\Lambda(\sigma)$ obtained using both a larger ensemble and a larger set of line elements.

From Fig. 1(a) it can be observed that Λ approaches a linear profile for large (positive or negative) values of σ. This tendency may be confirmed by examining the behavior of the midpoint derivative of Λ, plotted in Fig. 1(b), that

TABLE I. Numerical values for $\bar{h}$ and $h_{\max}$ for different values of A. Also shown in parenthesis the theoretical estimates for $\bar{h}$ [see Eq. (38)] and an upper bound for $h_{\max}$ [see Eq. (39)].

A	$\pi/2$	π	2π
$\bar{h}$	0.3 (0.31)	1.1 (1.09)	2.33 (2.31)
$h_{\max}$	1.28 (1.34)	2.24 (2.43)	3.57 (3.71)

beyond a range of values of σ, its value saturates (an exception being the case of $A=\pi/2$ for which a larger range of values of σ would be necessary to see this). This behavior is of no surprise given that the slope of Λ is controlled by the value of h. As the value of σ decreases (starting from $\sigma=0$), the value of Λ' increases until it reaches its largest value, $h_{\max}$. Note that for these values of σ, the numerically obtained Λ' is observed to be "wiggly." This is because these values of Λ' are associated with values of h near $h_{\max}$ which occur extremely infrequently. Thus, in order to obtain a Λ' that is less wiggly, both a larger ensemble and a larger set of line elements, would be necessary. However, the current precision is sufficient for calculating the smaller order scaling exponents, particularly $\tilde{\gamma}_1$ and $\tilde{\gamma}_2$ which are the main focus of this paper. For these cases, the regimes of interest are $-2 < \sigma_1 \le -1$ ($\tilde{\gamma}_1 < 1$) and $-3 < \sigma_2 \le -1$ ($\tilde{\gamma}_2 < 2$).

The appearance of a saturated Λ' indicates that Λ is resolved for (almost) all possible range of values of h. This is confirmed by comparing the numerical values for $h_{\max}$ with its upper bound (see Table I). Note the close agreement between the theoretical and numerical values for $\bar{h}$. Note also that because the saturation is reached faster for larger A, the values of $\bar{h}$ and $h_{\max}$ lie closer to each other.

1. Crámer function

To determine $\tilde{\gamma}_q$ it is not necessary to evaluate the Crámer function [see Eq. (34)]. Nevertheless, it is interesting to calculate $G(h)$ and examine how it varies with the flow characteristics. This calculation readily follows from Eq. (33). The resulting curve, plotted for positive values of h, is shown in Fig. 2.
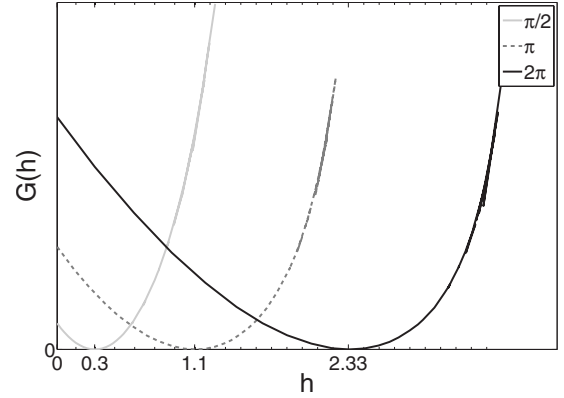
FIG. 2. The Crámer function $G(h)$ corresponding to the alternating sine flow [Eq. (36)] for $A=\pi/2$, π and 2π ($\tau=1$).

The shape of $G(h)$ is strongly dependent on the shear strength of the flow. In particular, as A increases, the chances for larger values of h to occur also increase, leading to a $G(h)$ that is increasingly skewed about $\bar{h}$ (see Fig. 2). Consequently, the region of h for which $G(h)$ is quadratic becomes smaller as A increases. Thus, approximating the scaling exponents with expression (35b), the usual approximation employed until now [9,11,12], is not sufficiently accurate. It will shortly be shown that the degree of inaccuracy depends on the values of both α and q.

2. Varying α

Using expression (34), the scaling exponents $\tilde{\gamma}_1$ and $\tilde{\gamma}_2$ are here computed and plotted as a function of α in Figs. 3 and 4 for the same values of A as before. As a means of comparison, γ_1 and γ_2 as well as $\tilde{\gamma}_1'$ and $\tilde{\gamma}_2'$ are also plotted in the same figures (discussion about results obtained from numerical simulations is postponed until Sec. IV B).

The results obtained confirm the conclusions of Sec. II. As is clearly depicted in Figs. 3 and 4, for $\alpha \to 0$ $\tilde{\gamma}_q = \gamma_q$, as predicted by Eq. (27). However, as α increases, $\tilde{\gamma}_q$ varies nonlinearly with α while $\tilde{\gamma}_q < \gamma_q$ for $\tilde{\gamma}_q < q$. In agreement with Eq. (28), the corrections, $\gamma_q - \tilde{\gamma}_q$, increase with α, reaching a maximum when $\alpha = \bar{h}$, the point at which the homogeneous-stretching approximation predicts a bulk
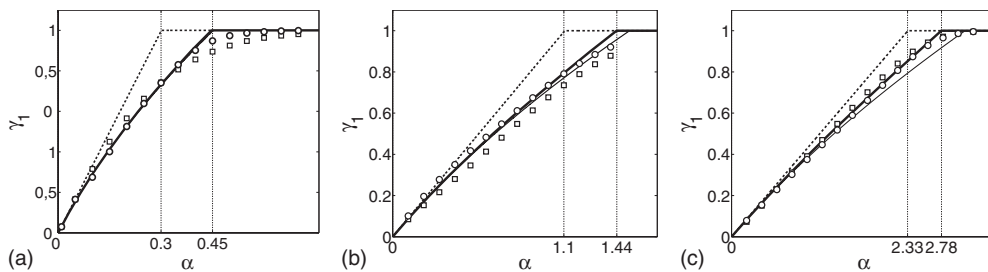
FIG. 3. The theoretical prediction for $\tilde{\gamma}_1$ [see Eq. (26)] is calculated using Eq. (34) and plotted against α for different values of A (thick solid line) for $\tau=1$. Also plotted γ_1 (dashed line), the homogeneous-stretching approximation [Eq. (1)] as well as $\tilde{\gamma}_1'$ (thin, solid line), the quadratic approximation [Eq. (35b)]. The theoretical results are in close agreement with the numerical results obtained from a set of simulations whereby an ensemble of 2000×2000 fluid parcels satisfying Eq. (7) are advected backward in time by Eq. (36) ($T=50\tau$). $\mathcal{F}$ is given by Eq. (3) and $\mathcal{F}_0(\boldsymbol{x})$ by Eq. (40). The scaling exponents are determined by calculating $S_1(\delta x)$ along a single intersection ($y=0$) and for two intervals: $10^{-5} < \delta x < 10^{-2}$ (squares) and $10^{-5} < \delta x < 10^{-4}$ (circles).
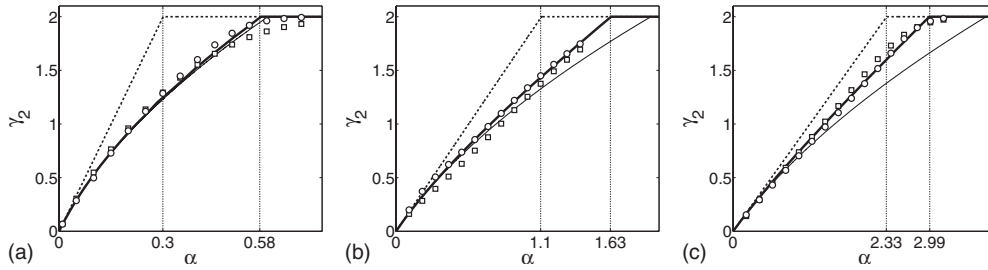
FIG. 4. Same as Fig. 3 but this time the focus is on the second-order scaling exponent ($\tilde{\gamma}_2$ (thick solid line), γ_2 (dashed line), and $\tilde{\gamma}'_2$ (thin solid line).

filamental-smooth transition to take place. As expected from expressions (29) and (30), the values of α for which $\gamma_1 = 1$ and $\gamma_2 = 2$, denoted by α_1^* and α_2^*, respectively, are both larger than $\bar{h}$ with $\alpha_2^* > \alpha_1^*$ (see also Table II).

The relative error induced by the homogeneous-stretching approximation when predicting the values of α_1^* and α_2^* can be measured in terms of $(a_1^* - \bar{h})/\bar{h}$ and $(a_2^* - \bar{h})/\bar{h}$, respectively. Its value depends on A, decreasing as A increases (see Table III). This is because the larger the value of A is, the more skewed $G(h)$ is with $\bar{h}$ and $h_{\max}$ becoming more akin to each other (see Fig. 2). In this case, the value of $h_{q\alpha}$ remains relatively close to $\bar{h}$ for all A rendering the relative error small.

Conversely, as A increases, $\tilde{\gamma}'_q$ becomes increasingly inaccurate with α. This inaccuracy becomes larger when $q=2$. This is because the value of $h_{q\alpha}$ increases with both q and α. Thus, for sufficiently large $h_{q\alpha}$, $G(h_{q\alpha})$ is no longer well approximated by Eq. (35a).

3. Varying q

During all previous work [9–12], the behavior of the scaling exponents were studied for a fixed value of α (usually $\alpha < \bar{h}/2$) and varying q. To put into context the results obtained here, $\tilde{\gamma}_q$, as well as γ_q and $\tilde{\gamma}'_q$, are calculated and plotted as a function of q for $\alpha = 0.25\bar{h}$ and $\alpha = \bar{h}$ in Figs. 5 and 6, respectively.

The results obtained confirm the conclusions of Sec. II. In both figures, for $q \to 0$, all three exponents are equal. However, as q increases, first γ_q, followed by $\tilde{\gamma}'_q$, start to deviate from $\tilde{\gamma}_q$. The deviation between $\tilde{\gamma}_q$ and γ_q increases monotonically with q with $\tilde{\gamma}_q < \gamma_q$. For values of α small compared to $\bar{h}$, this deviation remains small (see Fig. 5), while for $\alpha = \bar{h}$ the deviation is larger (see Fig. 6). In addition to α, the magnitude of the deviation also depends on the value of

A. The larger the value of A is, the closer the values of $\bar{h}$ and $h_{\max}$ are, leading a smaller difference between $\tilde{\gamma}_q$ and γ_q.

Similarly, the deviation between $\tilde{\gamma}_q$ and $\tilde{\gamma}'_q$ increases with q (see Figs. 5 and 6). This is because the larger q is, the larger $h_{q\alpha}$ is [see Eq. (23)]. If α is chosen to be sufficiently small, as is the case in Fig. 5, the value of $h_{q\alpha}$ remains close to $\bar{h}$ within a range of values of q (in Fig. 5 $q \le 5$). On the other hand, for larger values of α, as is the case in Fig. 6, $h_{q\alpha}$ is no more within the immediate neighborhood of $\bar{h}$ and thus for a skewed $G(h)$ the deviation is large even for small values of q. The case of $A = \pi/2$ is excluded, as in this case $G(h)$ is well approximated by a parabola for the range of $h_{q\alpha}$ considered.

In Sec. II we deduced that for large q, $\tilde{\gamma}_q$ should exhibit a linear dependence on q with the value of $\tilde{\gamma}_q/q$ controlled by the value $\alpha/h_{\max}$ [see Eq. (32)]. This linear dependence is clearly depicted in Figs. 5 and 6 where a line of slope $\alpha/h_{\max}$ is plotted against q for $q \ge 4$. The dependence is less prominent in Figs. 5(a) and 6(a) where higher values of q would be necessary to attain the large-q linear behavior.

The large-q linear behavior of $\tilde{\gamma}_q$ should be contrasted with the large-q $q^{1/2}$ dependence of the scaling exponents obtained for a quadratic Crámer function. For the alternating sine flow [Eq. (36)] or indeed any flow of finite velocity gradient ($\nabla \mathbf{v}$), $G(h)$ is quadratic only within a region around $\bar{h}$ while it necessarily has an $h_{\max}$.

B. Simulations

In order to support the theoretical considerations made in Sec. II and to provide a direct comparison with the results obtained in Sec. IV A, we here show a set of numerical simulations obtained for a variety of values of α and the same values of A as before. The stationary-state chemical fields are reconstructed by following backward in time an ensemble of fluid parcels with the source $\mathcal{F}_0$ given by

TABLE II. Numerical estimates for $\bar{h}$, α_1^*, and α_2^* for different values of A.

A	$\pi/2$	π	2π
$\bar{h}$	0.3	1.1	2.33
a_1^*	0.45	1.44	2.78
a_2^*	0.58	1.63	2.99

TABLE III. The relative error induced by the homogeneous-stretching approximation when predicting the values of α_1^* and α_2^* for different values of A.

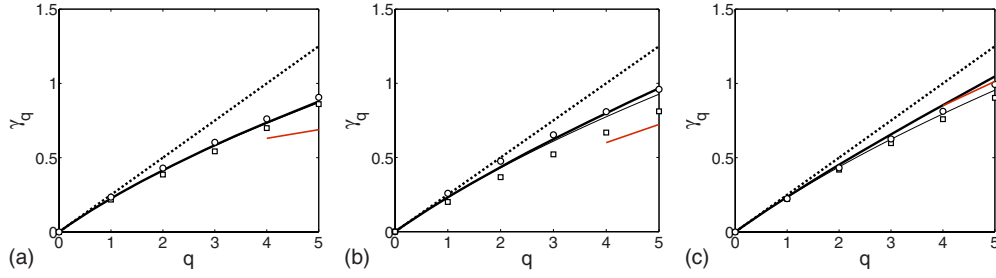| A	$\pi/2$	π	2π
$(a_1^* - \bar{h})/\bar{h}$	0.5	0.31	0.19
$(a_2^* - \bar{h})/\bar{h}$	0.93	0.48	0.28

FIG. 5. (Color online) Same as Fig. 3 where this time the scaling exponents are plotted as function of q for $\alpha=0.25\bar{h}$ so that $\gamma_q=0.25q$ (dashed black line) [see Eq. (1)]. Also plotted $\tilde{\gamma}_q$ [see Eq. (26)—thick solid black line] and $\tilde{\gamma}'_q$ [see Eq. (35b)—thin solid black line]. A line in solid light gray (red) of slope equal to $\alpha q/h_{max}$ is plotted for large q [see also Eq. (32)].

$$\mathcal{F}_0(\boldsymbol{x}) = 1/2\{1 - \cos[2\pi(x+y)]\}. \qquad (40)$$

As before, $\boldsymbol{v}(\boldsymbol{x},t)$ is given by Eq. (36). By making the following variable transformation,

$$\hat{C}_{X(t)}(t) = C_{X(t)}(t)e^{\alpha t} - c(\boldsymbol{x},0), \qquad (41a)$$

Equation (7a) is transformed into

$$\frac{d\hat{C}_{X(t)}(t)}{dt} = \alpha\mathcal{F}_0(\boldsymbol{X}(t))e^{\alpha t}, \qquad (41b)$$

Thus, to obtain $c(\boldsymbol{x},0)$, Eq. (41b) can be integrated at the same time as the parcel trajectories are followed backward in time up to some time $t=-T$. Note that $\hat{C}(0)=0$ [recall Eq. (8)]. Thereafter, knowing $\hat{C}(-T)$, $c(\boldsymbol{x},0)$ is readily obtained from Eq. (41a), where for sufficiently large T, the term in C vanishes. The novelty of this method is that it allows higher field resolutions, with the resolution unconstrained by computer limitations (e.g., computer memory), while at the same time, significantly reducing the total computation length.

At first we concentrate on the chemical fields obtained for various values of α and $A=\pi/2$ (see Fig. 7). The system is let to evolve for a time $T=50\tau$, where $\tau=1$. This value of T is large enough to ensure that a statistical equilibrium will be reached for all values of α. The field's resolution is 2000×2000, achieved by following this many fluid parcels with their final positions fixed on a square grid. The integration is carried out using a second-order Runge-Kutta method with time step $\delta t=0.01$. In all cases, the same sequence of flow angles ϕ_1 and ϕ_2 is used.

The values of α depict six cases of interest. The first case, $\alpha=0.1<\alpha_1^*$ ($\tilde{\gamma}_1=0.23$), corresponds to the typical filamental behavior for the chemical field [see Fig. 7(a)]. The second case, $\alpha=0.3<\alpha_1^*$ ($\tilde{\gamma}_1=0.73$), corresponds to the value of $\alpha=\bar{h}$ for which the homogeneous-stretching approximation predicts a bulk filamental-smooth transition to take place. Instead, the chemical field is clearly filamental [Fig. 7(b)]. The third and fourth cases [Figs. 7(c) and 7(d)], $\alpha=0.35$ ($\tilde{\gamma}_1=0.83$) and $\alpha=0.4$ ($\tilde{\gamma}_1=0.92$), respectively, correspond to $\bar{h}<\alpha<\alpha_1^*$ while the fifth and sixth cases [Figs. 7(e) and 7(f)] correspond to $\alpha=\alpha_1^*$ and $\alpha=0.6>\alpha_1^*$ (both with $\tilde{\gamma}_1=1$), respectively. Although the overall behavior of the field is smooth, there still exist some isolated filamental regions which become increasingly isolated as α increases until $\alpha>h_{max}$ at which point these filamental regions should cease to exist. Note that, for this example, $h_{max}=1.28$ (see Table I). It is therefore difficult to distinguish a single value of α for which one can say that the field becomes smooth on a macroscopic scale.

The first- and second-order scaling exponents are determined from the structure functions calculated along a single intersection ($y=0$) and over two intervals for δx: $10^{-5}<\delta x<10^{-4}$ and $10^{-5}<\delta x<10^{-2}$ [see Figs. 3 and 4]. The agreement between theory and numerics is very good, especially for the exponents obtained within the first space interval. This is expected since the smaller the value of δx is, the more accurate is the approximate expression for the finite-size Lyapunov exponent distribution [Eq. (16)] from which $\tilde{\gamma}_q$ is deduced. However, the agreement is less good in the neighborhood of α_1^* (Fig. 3) and α_2^* (Fig. 4). The reason for this is not fully understood. Its origin may lie in the contribution of higher-order terms when using Laplace's
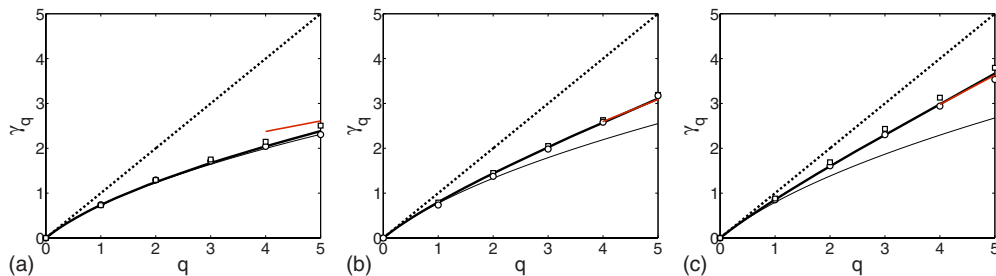

FIG. 6. (Color online) Same as Fig. 5 but this time $\alpha=\bar{h}$ so that $\gamma_q=q$ (dashed black line) [see Eq. (1)]. A line in solid light gray (red) of slope equal to $\alpha q/h_{max}$ is plotted for large q [see also Eq. (32)].
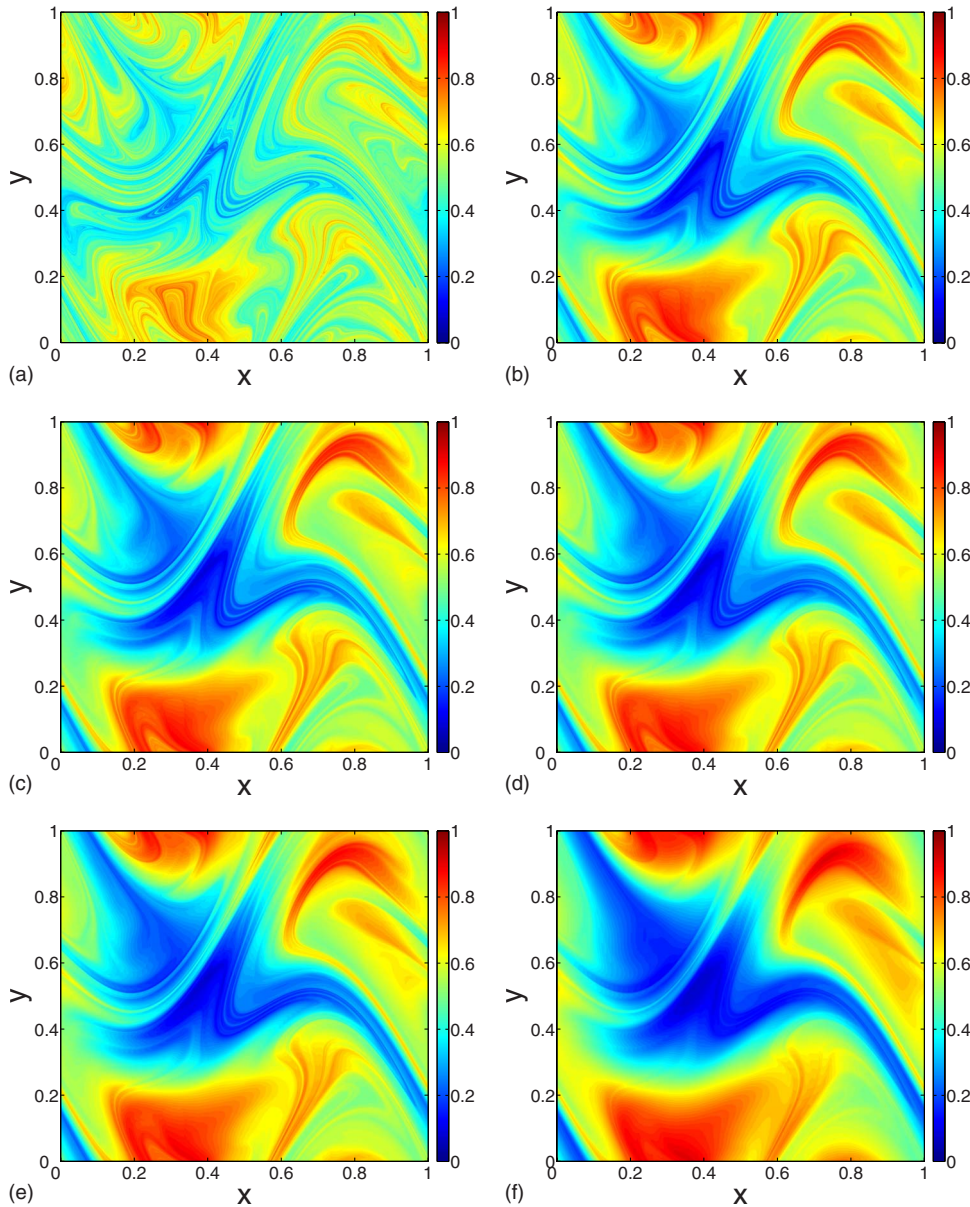
FIG. 7. (Color online) Snapshots of the reactive field at statistical equilibrium ($T=50\tau$) for various values of α ($A=\pi/2$). Case (b) corresponds to the value of α for which the homogeneous-stretching approximation predicts a bulk filamental-smooth transition. The color bars on the right of each graph give the concentration values associated with the different colors.

method. Nevertheless, this discrepancy is certainly length scale dependent. In a similar way, we determine the higher-order scaling exponents (see Figs. 5 and 6). Again, the agreement between theory and numerics is very good, especially for the exponents obtained within the interval that involves smaller length scales.

V. SUMMARY AND CONCLUSIONS

In this paper we have analyzed, in the large-Péclet limit, the small-scale spatial structure of a linearly decaying chemical field generated by a chaotic-advection flow and sustained by a large-scale spatially smooth source. As has been identified previously [7,9–12], for sufficiently slow chemical processes, the spatial structure of the chemical field is filamental; as the chemical processes become faster, the spatial structure becomes progressively smoother. Our aim in this paper has been to investigate in detail the variation in the

spatial structure of the chemical field with the chemical decay rate, α, paying particular attention to the filamental-smooth transition. Initially focusing on the local singularities of the chemical field as measured by the Hölder exponent, we examined its average scaling behavior as quantified by the scaling exponents of its qth-order structure functions.

In agreement with previous work [7,9–12], we found that the scaling exponents depend both on α and on the stretching properties of the flow. However our focus on the variation in α emphasizes that the inhomogeneity in stretching plays an important role even for moderate values of q, as shown in Figs. 3 and 4, for example, for $q=1$ and $q=2$, where the strong deviation from the homogeneous-stretching approximation is clearly visible. (Previous work has tended to emphasize variation with q, e.g., our Fig. 5, where the deviation from the homogeneous-stretching approximation appears small for moderate values of q.) Our conclusion is that the homogeneous-stretching approximation is good only for vanishingly small values of α and q. The inhomogeneous

stretching can be included via the Crámer function that encapsulates the finite-time stretching statistics of the flow. The relevance of the Crámer function was established after a careful investigation of the relation between finite-time and finite-size Lyapunov exponents, where the latter governs the spatial properties of the chemical field. We found that the corrected scaling exponents, $\widetilde{\gamma}_q$, depend nonlinearly on α and are smaller than γ_q, the exponents predicted by a homogeneous-stretching approximation. As α increases, so does the magnitude of the correction to the homogeneous-stretching approximation, $\gamma_q - \widetilde{\gamma}_q$, reaching a maximum when $\alpha = \bar{h}$, the point at which the homogeneous-stretching approximation predicts a bulk filamental-smooth transition to take place [see Eq. (28)]. Examining the behavior of the scaling exponents as a function of α and q we identified the following regimes:

(i) For $\alpha \leq \bar{h}$, $\widetilde{\gamma}_q < q$ for all q [see Eq. (29)]. In this regime the chemical field can be unambiguously described as filamental. Neufeld *et al.* [9] had already identified this regime as one in which the set of points on which the Hölder exponent is less than 1 is space-filling.

(ii) For $\bar{h} < \alpha < h_{\max}$, there exists a $q_0 > 0$ such that $\widetilde{\gamma}_q = q$ for $q \leq q_0$ and $\widetilde{\gamma}_q < q$ for $q > q_0$. The value of q_0 depends on α, increasing with α, and satisfies $q_0 = 0$ when $\alpha = \bar{h}$ and $q_0 \to \infty$ as $\alpha \to h_{\max}^-$, where $h_{\max}$ denotes the maximum finite-time stretching rate [see Eq. (31)]. Neufeld *et al.* [9] described this regime as one in which the set of points on which the Hölder exponent is less than 1 has a fractal dimension that is less than 2 where 2 is the dimension of the domain. In this regime the chemical field can be described as having an intermediate character.

(iii) For $\alpha > h_{\max}$, $\widetilde{\gamma}_q = q$ for all q, i.e., the chemical field can be described as unambiguously smooth.

The implication is that there is no sharp bulk filamental-smooth transition. Instead the transition takes place over a finite range of α corresponding to regime (ii). This is confirmed by the numerical results shown in Fig. 7 where no clear sharp transition is visible.

The good agreement between the theoretical and numerical results obtained in this paper confirmed the approach followed and the conclusions reached. The comparison between theory and numerics was achieved by careful calculation of the Crámer function for a particular type of renewing flow, the alternating sine flow. This calculation allowed as to explore regions where the Crámer function is not described by a Gaussian approximation. One important implication of this approximation is that it neglects the existence of a maximum finite-time stretching rate $h_{\max}$ and therefore misses regime (iii). Additionally, it predicts incorrect large-q asymptotics for $\widetilde{\gamma}_q$ in regimes (i) and (ii). Neufeld *et al.* [9] have previously noted this point. However, their expression for large-q asymptotics for $\widetilde{\gamma}_q$ (Eq. (4.15) in Ref. [9]) cannot be correct since $G(h)$ is singular at $h = h_{\max}$ (and not defined for $h > h_{\max}$) (see Fig. 2). In regimes (i) and (ii) it is the case that for all q, $\widetilde{\gamma}_q > q\alpha/h_{\max}$ and it may be shown [see Eq. (32)] that $\widetilde{\gamma}_q \sim q\alpha/h_{\max}$ becomes a better approximation as q increases (in the sense that the relative error tends to zero).

Although the model that we considered is highly simplified, it can be extended to include multiply interacting chemical fields. In this case, in addition to the stretching exponent distribution, the theoretical development should incorporate a distribution of chemical Lyapunov exponents. Our analysis has concentrated on cases for which the characteristic length scale of the source, $L_{\mathcal{F}_0}$, is equal to the characteristic length scale of the flow, L_v. Because the spatial structure depends on the recent stretching history of the flow, our analysis should continue to hold for cases for which $L_{\mathcal{F}_0} > L_v$. Note that for an unforced chemical field, $L_{\mathcal{F}_0} \approx L_v$ and $L_{\mathcal{F}_0} \gg L_v$ are two very different cases (see Ref. [37] for more details).

The results of this paper emphasize the stretching statistics of the flow, not just the mean stretching rate, have an important effect on the stationary-state average scaling behavior of the chemical field. Sufficiently accurate calculations of the stretching statistics of the flow have only recently become possible in both experiments [38,39] and observations of the surface ocean flow [6,40]. We therefore anticipate that interpretations of future experiments and observations will benefit from our conclusions.

APPENDIX

1. Finite-size versus finite-time statistics

a. General argument to capture the long-time behavior of the first-passage-time distribution

Consider the general relation between $p(0,t)$ and $q_0(t)$, given by Eq. (17), repeated here:

$$p(0,t) = \int_0^t q_0(t') p_0(t - t') dt'. \tag{A1}$$

The large-t behavior of $q_0(t)$ can be obtained by considering the following argument. For a large value of z_0 it is useful to rescale t and t' by $t = z_0 \tau$ and $t' = z_0 \tau'$, respectively, where τ and τ' are formally $O(1)$. We now substitute the large deviation form for $p(z,t)$ and $p_0(t)$ into Eq. (A1) [see Eq. (15) but now applied to the random walk] to obtain

$$\exp[-z_0 \tau G(1/\tau)] \propto \int_0^\tau q_0(z_0, \tau') \exp[-z_0(\tau - \tau')G(0)] d\tau'. \tag{A2}$$

A leading-order approximation for $q_0(t)$ can be deduced using Laplace's method, valid for large z_0. There exist two

possibilities: The first possibility is that the integral is dominated by $\tau' = \tau$ in which case

$$q_0(z_0\tau) \propto \exp[-z_0\tau G(1/\tau)]. \tag{A3a}$$

The second possibility is that the integral is dominated by $\tau' = \sigma < \tau$ in which case

$$q_0(z_0\sigma) \propto \exp[z_0(\tau - \sigma)G(0) - z_0\tau G(1/\tau)]. \tag{A3b}$$

We now examine which possibility is viable. The first possibility is self-consistent. Since G is a convex function and $\tau' < \tau$,

$$\tau G(1/\tau) < \tau' G(1/\tau') + (\tau - \tau')G(0). \tag{A4}$$

Hence, for $q_0(z_0\tau)$ satisfying Eq. (A3a), the integrand in Eq. (A2) has a maximum at $\tau' = \tau$. The second possibility leads to a contradiction. To see this consider Eq. (A3b). Its right-hand side should be independent of τ. But this cannot be true as this would imply that for all τ, $G(0) = G(1/\tau)$. We therefore deduce that the correct leading order approximation for $q_0(t)$ is given by Eq. (A3a) and thus, the long-t behavior of $q_0(t)$ is given by

$$q_0(t) \propto \exp[-tG(z_0/t)], \quad \text{for } z_0 \gg 0. \tag{A5}$$

b. Connection with the diffusion-drift problem

Consider a particle undergoing a simple random walk with a constant drift and diffusion. Let $p(z,t)$ be the *pdf* associated with the probability that the particle is at point z at time t, given that it was at $-z_0 < 0$ at $t=0$. The corresponding Fokker-Planck equation (FPE) is given by

$$\partial_t p(z,t) + u_0\partial_z p(z,t) = D\partial_z^2 p(z,t), \tag{A6a}$$

with $u_0, D > 0$ the drift velocity and kinematic diffusion coefficient, respectively. The FPE (A6a) is equivalent [41] to the following Langevin equation:

$$\dot{Z}(t) = u_0 + \xi(t), \tag{A6b}$$

where $\xi(t)$ is a white noise, i.e., $\overline{\xi(t)} = 0$ and $\overline{\xi(t)\xi(t')} = 2D\delta(t-t')$, with the bar denoting a temporal average and the dot a derivative. Note that for $Z(t) = \ln(X(t))$ and $D = u_0/d$, where d is the dimension of the domain, the Langevin Eq. (A6b) describes the evolution of parcel pair distance, $\delta X(t)$, in an isotropic Kraichnan flow [35].

It is easy to calculate the *pdf* associated with the first-passage-time probability, $q_0(t)$, i.e., $q_0(t)\delta t$ is the probability that $Z(t) = 0$ for the first time during the interval $[t, t+dt]$. The FPE (A6a) has the following solution:

$$p(z,t) = \frac{1}{\sqrt{4\pi Dt}}\exp\left[-\frac{t}{4D}\left(\frac{z+z_0}{t} - u_0\right)^2\right]. \tag{A7}$$

To determine $q_0(t)$, consider $\tilde{p}(z < 0, t)$, where $\tilde{p}(z < 0, t)$ is the solution of Eq. (A6a) in the presence of an absorbing boundary such that $\tilde{p}(0,t) = 0$ for all $t > 0$. A standard result [30] is that

$$\tilde{p}(z,t) = p(z,t)\left(1 - \exp\left[\frac{zz_0}{Dt}\right]\right). \tag{A8}$$

It can be deduced [30,41] that

$$q_0(t) = -\partial_t\int_{-\infty}^{0}\tilde{p}(z,t)dz \tag{A9a}$$

$$= -D\partial_z\tilde{p}(z,t)\big|_{z=0} = \frac{Dz_0}{t}p(0,t) \tag{A9b}$$

$$= \frac{z_0}{\sqrt{4\pi Dt^3}}\exp\left[-\frac{t}{4D}\left(\frac{z_0}{t} - u_0\right)^2\right]. \tag{A9c}$$

Determining $Q(h, \delta x)$, the *pdf* for the FSLEs, is analogous to determining the distribution of the particle's average velocity over the period until it first visits the origin. Let this velocity be denoted by $V(t)$. Its distribution, $Q(v, z_0)$, can be determined from $q_0(t)$ by a change of variables, $V(t) = z_0/T$, where T denotes the first-passage time. This results into

$$Q(v,z_0) = \frac{z_0}{v^2}q_0(t = z_0/v) = \frac{1}{\sqrt{4\pi Dz_0v}}\exp\left[-\frac{z_0(v-u_0)^2}{4Dv}\right]. \tag{A10}$$

Determining $P(h,t)$ is analogous to determining the distribution of the average particle velocity (averaged over all times prior to t). Let this velocity be denoted by $U(t)$. Its distribution, denoted by $P(u,t)$, can be obtained from $p(z,t)$ [see Eq. (A7)] by a change of variables $U(t) = (Z(t)+z_0)/t$ which leads to

$$P(u,t) = tp(z = ut - z_0, t) = \sqrt{\frac{t}{4\pi D}}\exp\left[-\frac{(u-u_0)^2t}{4D}\right]. \tag{A11}$$

Approximation (16) is equivalent to setting $t = z_0/u$ and $u = v$ in Eq. (A11) from where we obtain that

$$Q \equiv Q_0. \tag{A12}$$

Thus, for this example of a one-dimensional diffusive random walk (a corresponding one-dimensional stretching process), approximation (16) is exact for all $z_0 > 0$.

2. Expression for the large-q behavior of $\tilde{\gamma}_q$

The large-q behavior of $\tilde{\gamma}_q$ can be obtained by considering $H(h) \equiv G(h)/h$, which is singular at h_{max}. From Eq. (26), the minimum of $q\alpha/h + H(h)$ occurs at $h = h_{q\alpha}$, where $h_{q\alpha}$ satisfies

$$H'(h_{q\alpha}) = q\alpha/h_{q\alpha}^2. \tag{A13a}$$

This implies that

$$H'(h_{q\alpha}) > q\alpha/h_{max}^2, \tag{A13b}$$

and thus, $H'(h_{q\alpha}) \to \infty$ as $q \to \infty$. Now consider $q\alpha/h_{q\alpha} + H(h_{q\alpha})$. First suppose that $H(h_{q\alpha})$ dominates the expression such that $H(h_{q\alpha}) > cq\alpha/h_{q\alpha}$, where $c > 0$ is some constant. Using Eq. (A13a) it follows that $H'(h_{q\alpha})/H(h_{q\alpha}) < c/h_{q\alpha}$ from where we can deduce that

$$H(h_{q\alpha}) < H(h_{1\alpha})\left(\frac{h_{q\alpha}}{h_{1\alpha}}\right)^c < H(h_{1\alpha})\left(\frac{h_{\max}}{h_{1\alpha}}\right)^c, \quad \text{(A14)}$$

i.e., $H(h_{q\alpha})$ is bounded as q increases. Equation (A14) is in contradiction with Eq. (A13b) as for a reasonable H, a bounded H implies a bounded H'. Therefore, for all $c > 0$, $H(h_{q\alpha}) < cq\alpha/h_{q\alpha}$. Using Eq. (25) we may thus deduce that for $\alpha < h_{\max}$,

$$\widetilde{\gamma}_q \sim \frac{\alpha q}{h_{\max}}, \quad \text{as } q \to \infty. \quad \text{(A15)}$$

3. Determining Λ

For a flow that is spatially homogeneous and random in time, Λ can be evaluated by considering the time-τ map of the flow, $\psi_{-\tau}$, that relates the fluid parcel positions at two times t and $t-\tau$ by $X(t-\tau) = \psi_{-\tau}X(t)$. As $X(t) \to 0$,

$$\delta X(t - \tau) = \nabla \psi_{-\tau}|_{X=0}\delta X(t) = S_{-\tau}\delta X(t), \quad \text{(A16)}$$

where τ denotes the time necessary for the flow to become uncorrelated and $S_{-\tau}$ is a random matrix with det $S_{-\tau} = 1$.

Let $p(\delta x, t)d\delta x$ be the probability that the value of $\delta X(t)$ lies between δx and $\delta x + d\delta x$ at time t. An approximate expression for $p(\delta x, t)$ may be deduced using its dependence on $P(h, t)$, whose large-deviation form was given in Eq. (15). $p(\delta x, t)$ may then be assumed to be proportional to both $P(h, t)$ as well as $q(\theta; h, t)$, a function weakly dependent on h and t that incorporates the dependence of the evolution of the line element on its orientation. Since $\delta x \propto e^{ht}$, a change of variables results in

$$p(\delta x, t) \sim \frac{1}{(\delta x)^2 t}P(h, t)q(\theta; h, t), \quad \text{(A17)}$$

where $\delta x = \delta x(\cos\theta, \sin\theta)$.

From Eq. (A16) it follows that $p(\delta x, t)$ obeys the following recurrence relation,

$$p(\delta x, t) = \int \langle \delta(S_{-\tau}\delta x - \delta x_{-\tau})\rangle p(\delta x_{-\tau}, t - \tau)d\delta x_{-\tau},$$

$$\text{(A18)}$$

where $\langle \ldots \rangle$ denotes averaging over the ensemble of random matrices and $\delta x_{-\tau} \equiv \delta x_{-\tau}(\cos(\theta_{-\tau}), \sin(\theta_{-\tau})) = S_{-\tau}\delta x$.

Once expression (A17) is substituted into Eq. (A18), the problem is at leading order transformed into a one-dimensional eigenvalue problem of the form

$$\langle \delta x_{-\tau}^{\sigma-1}q(\theta_{-\tau})\rangle = \nu(\sigma)\delta x^{\sigma-1}q(\theta), \quad \text{(A19a)}$$

with

$$\sigma = -[1 + G'(h)] \text{ and } \nu(\sigma) = \exp(-\tau[G(h) - hG'(h)]).$$

$$\text{(A19b)}$$

The eigenvalue $\nu(\sigma)$ can now be numerically determined for a range of values of σ by evaluating Eq. (A19) for an ensemble of random matrices $S_{-\tau}$. The function $\Lambda(\sigma)$ is then obtained using the relation

$$\Lambda(\sigma) = -\ln[\nu(\sigma)]/\tau. \quad \text{(A20)}$$

[1] H. Aref, J. Fluid Mech. **143**, 1 (1984).

[2] H. Aref, Phys. Fluids **14**, 1315 (2002).

[3] J. M. Ottino, *The Kinematics of Mixing: Stretching, Chaos, and Transport* (Cambridge University Press, Cambridge, England, 1989).

[4] S. Wiggins, *Chaotic Transport in Dynamical Systems* (Springer, New York, 1992).

[5] E. Ott, *Chaos in Dynamical Systems* (Cambridge University Press, Cambridge, England, 1993).

[6] E. Abraham and M. M. Bowen, Chaos **12**, 373 (2002).

[7] Z. Neufeld, C. López, and P. H. Haynes, Phys. Rev. Lett. **82**, 2606 (1999).

[8] K. Nam, T. M. Antonsen, P. N. Guzdar, and E. Ott, Phys. Rev. Lett. **83**, 3426 (1999).

[9] Z. Neufeld, C. López, E. Hernández-García, and T. Tél, Phys. Rev. E **61**, 3857 (2000).

[10] G. Boffetta, A. Celani, S. Musacchio, and M. Vergassola, Phys. Rev. E **66**, 026304 (2002).

[11] Y. K. Tsang, E. Ott, T. M. J. Antonsen, and P. N. Guzdar, Phys. Rev. E **71**, 066313 (2005).

[12] I. J. Benczik, Z. Neufeld, and T. Tél, Phys. Rev. E **71**, 016208 (2005).

[13] M. Chertkov, Phys. Fluids **10**, 3017 (1998).

[14] E. Hernández-García, C. López, and Z. Neufeld, Chaos **12**, 470 (2002).

[15] D. A. Birch, Y. K. Tsang, and W. R. Young, Phys. Rev. E **75**, 066304 (2007).

[16] E. R. Abraham, Nature (London) **391**, 577 (1998).

[17] A. Tzella and P. H. Haynes, Biogeosciences **4**, 173 (2007).

[18] A. Tzella and P. H. Haynes, Phys. Fluids **21**, 087101 (2009)

[19] R. T. Pierrehumbert, Chaos, Solitons Fractals **4**, 1091 (1994).

[20] Z. Neufeld, P. H. Haynes, and G. Picard, Phys. Fluids **12**, 2506 (2000).

[21] C. López and E. Hernández-García, Eur. Phys. J. B **28**, 353 (2002).

[22] C. M. Bender and S. A. Orszag, *Advanced Mathematical Methods for Scientists and Engineers: Mathematical Series* (McGraw-Hill, New York, 1978).

[23] G. Lapeyre, Chaos **12**, 688 (2002).

[24] V. I. Oseledec, Trans. Mosc. Math. Soc. **19**, 197 (1968).

[25] E. Aurell, G. Boffetta, A. Crisanti, G. Paladin, and A. Vulpiani, J. Phys. A **30**, 1 (1997).

[26] G. Artale, A. Boffetta, A. Celani, M. Cencini, and A. Vulpiani, Phys. Fluids **9**, 3162 (1997).

[27] R. S. Ellis, *Entropy, Large Deviations, and Statistical Mechanics* (Springer-Verlag, New York, 1985).

[28] H. Crámer, Actualités Scientifiques et Industrielles **736**, 5 (1938).

[29] U. Frisch, *Turbulence* (Cambridge University Press, Cam-

bridge, England, 1995).

[30] S. Redner, *A Guide to First-passage Processes*, 1st ed. (Cambridge University Press, Cambridge, England, 2007).

[31] T. M. J. Antonsen, Z. Fand, E. Ott, and E. Garcia-López, Phys. Fluids **8**, 3094 (1996).

[32] D. R. Fereday and P. H. Haynes, Phys. Fluids **16**, 4359 (2004).

[33] P. H. Haynes and J. Vanneste, Phys. Fluids **17**, 097103 (2005).

[34] J. Vanneste (unpublished).

[35] R. H. Kraichnan, Phys. Fluids **11**, 945 (1968).

[36] T. Bohr and D. Rand, Physica D **25**, 387 (1987).

[37] Y.-K. Tsang, Phys. Rev. E **80**, 026305 (2009).

[38] M. Giona, S. Cerbelli, and A. Adrover, Phys. Rev. Lett. **88**, 024501 (2001).

[39] P. E. Arratia and J. P. Gollub, Phys. Rev. Lett. **96**, 024501 (2006).

[40] D. W. Waugh and E. R. Abraham, Geophys. Res. Lett. **35**, L20605 (2008).

[41] C. W. Gardiner, *Handbook of Stochastic Methods: For Physics, Chemistry, and the Natural Sciences*, Springer Series in Synergetics (Springer, New York, 1996).

[42] Note that Boffetta *et al.* [10] refer to the stir-down time as the exit time.